06

The influence of nanocomposites on the memristive properties of $Cu/(Co_{40}Fe_{40}B_{20})_x(SiO_2)_{100-x}/LiNbO_3/Cr/Cu/Cr$ capacitor structures

© A.V. Sitnikov,[1,2] Yu.E. Kalinin,[1] I.V. Babkina,[1] A.E. Nikonov,[1] D.S. Pogrebnoy,[1] A.R. Shakurov[1]

[1] Voronezh State Technical University,
394026 Voronezh, Russia
[2] National Research Center „Kurchatov Institute“,
123182 Moscow, Russia
e-mail: Aleks.shakurov@mail.ru

Received February 21, 2025
Revised May 19, 2025
Accepted June 18, 2025

The paper reveals the results of a study of the memristive properties of the $Cu/(Co_{40}Fe_{40}B_{20})_x(SiO_2)_{100-x}/LiNbO_3/Cr/Cu/Cr/citall$ structure. It has been shown that the use of $(Co_{40}Fe_{40}B_{20})_x(SiO_2)_{100-x}$ nanocomposites makes it possible to realize a set of good, practically significant memristive properties. Thus, the switching voltage from the HRS to the LRS state of the capacitor structure and back is ± 4 V, the R_{off}/R_{on} ratio reaches hundreds of units, the number of reversible resistive switching cycles is more than 10^4, and the plasticity of resistive states are being realized. It has been confirmed that to implement a multifilament resistive switching in a dielectric layer, the presence of nanocomposite in the concentration range of the metal phase up to the percolation threshold is necessary as an upper electrode. In this case, the main role is played by the structure of the nanocomposite, and the elemental composition of the heterogeneous film is not so significant for the implementation of a complex of technologically significant properties of the memristor.

Keywords: Resistive switching, memristors, nanocomposite, lithium niobate.

DOI: 10.61011/TP.2025.11.62237.25-25

Introduction

The intensive development of artificial intelligence in recent years has put forward certain requirements for the development of a new electronic component base. In this regard, one of the promising areas of research is metal-dielectric-metal (M/D/M) memristive structures, where the effect of reversible resistive switching (RS) has been detected. This property can be used both to create elements of non-volatile multilevel memory and to emulate synapses in the development of neuromorphic computing systems that are effective in solving artificial intelligence tasks: natural language and image recognition, decision making, generalization, forecasting, etc. [1–8].

Reversible RS can, in most cases, be explained by two mechanisms of changing the processes of electrical transfer. In the first case, the electromigration of oxygen vacancies in a dielectric layer under the action of a high electric field strength is considered [1,7]. In the second case, the penetration of metal cations (for example, Cu, Ag) into a dielectric of electrodes of the appropriate composition [2,8–13]. As a result of these processes, thin conductive channels (filaments) are created or destroyed in the dielectric layer, which determine the resistive characteristics of the functional layer. Obviously, with a low density of such channels, their position and the stress of synthesis and destruction are largely determined by defects in the memristive structure. This largely random mechanism of formation of conductive channels causes a wide variation in characteristics from element to element and a high degree of degradation of the properties of memristors in case of cyclic RS [1,2].

We proposed the use of a metal-dielectric nanocomposite (NC) film as one of the electrodes. The electrotransport is carried out along a chain of metal nanogranules in NC up to the percolation threshold. These channels determine the spatial location and surface concentration of the filaments in the dielectric layer. The chosen approach was tested in memristive structures of M/NC/M, where NC was a heterogeneous system $(Co_{40}Fe_{40}B_{20})_x(LiNbO_3)_{100-x}$. In this case, the possibility of implementing bipolar resistive switching with the ratio of high-resistance (R_{off}) to low-resistance (R_{on}) resistive states $R_{off}/R_{on} \approx 100$ was shown [14–16]. In addition, for this structure, the endurance (number of RS cycles) exceeded 10^6, and the retention time of resistive states was 10^4 s [15,16]. Memristive elements also showed the possibility of a smooth change in the resistive state in the $R_{off} - R_{on}$ window (plasticity), and this made it possible to emulate important properties of biological synapses [16–19]. Structural studies of the memristive element $M/(Co_{40}Fe_{40}B_{20})_x(LiNbO_3)_{100-x}/M$) have shown that at the initial stage of nanocomposite growth, a dielectric is formed on the lower metal electrode as a result of the self-organization process interlayer ($LiNbO_3$) with a thickness of 10−15 nm [20,21]. In this regard, M/NC/D/M structures were synthesized, where a $LiNbO_3$ layer with a thickness

of 10−15 nm is used as the D. The resulting structures had properties similar to those shown above.

Supposition on formation of multi-filament RS in structures M/NC/D/M due to conductive channels of NC provide high degree of variation in properties optimization due to use of NC with different composition of metallic and dielectric phases. The most studied nanocomposite is $(Co_{40}Fe_{40}B_{20})_x(SiO_2)_{100-x}$ which, from one hand has homogeneous nanogranular structure [22], and on the other hand rather high thermal stability of structural and electrical properties [23].

Therefore, the main purpose of this study is to identify the effect of the dielectric phase of the nanocomposite $(Co_{40}Fe_{40}B_{20})_x$

1. Specimens and study methods

Memristive structures $Cu/(Co_{40}Fe_{40}B_{20})_x(SiO_2)_{100-x}/LiNbO_3$/Cr-Cu-Cr/polycrystalline glass (Fig. 1) were obtained by ion beam spraying using shadow masks.

At the first stage, the lower electrode of the Cr–Cu–Cr 100/1000/100 nm structure was deposited, respectively. The ion purification of the substrate surface was performed before the deposition of the metal film. The synthesis was carried out in one technological cycle by sequential sputtering of Cr and Cu targets at an anode voltage of 2 kV and a plasma current of 100 mA at a pressure of Ar $3.9 \cdot 10^{-4}$ Torr. The choice of a multilayer configuration of the metal electrode allows, on the one hand, protecting the copper film from the impact of the natural oxidation process in the atmosphere, on the other hand, creating a buffer layer that prevents the processes of electromigration of Cu ions into the NC film, forming an electrode with a low electrical resistivity at the same time.

Subsequent sputtering of films

$$(Co_{40}Fe_{40}B_{20})_x(SiO_2)_{100-x}/LiNbO_3$$

(for brevity, we will denote the composite $(Co_{40}Fe_{40}B_{20})_x(SiO_2)_{100-x}$ in this structure as $(CoFeB)_x(SiO_2)_{100-x}$) was carried out through shadow masks on four Cr–Cu–Cr/polycrystalline glass substrates arranged in a row so that the total area of the working surface was 240 × 48 mm. The shadow screen covered the substrates and had holes with a diameter of 8 mm, arranged in 24 rows of 6 holes per row. $LiNbO_3$ film was deposited as follows. The target was a plate of single-crystal lithium niobate with a size of 280 × 80 × 2 mm, secured on a water-cooling base. Spraying was carried out in an Ar atmosphere at a pressure of $3.9 \cdot 10^{-4}$ Torr with the addition of $1.9 \cdot 10^{-5}$ Torr O_2, which made it possible to reduce the oxygen deficiency in the synthesized film. $LiNbO_3$ was deposited onto the substrate in the mode of its passage in the spray position. The speed of movement of the substrate was set by the speed of rotation of the carousel of the substrate holder (one revolution for 5 min). The deposited coating thickness was about 5 nm in one cycle. There were three such deposition cycles, and the total thickness of lithium niobate was about 15 nm.

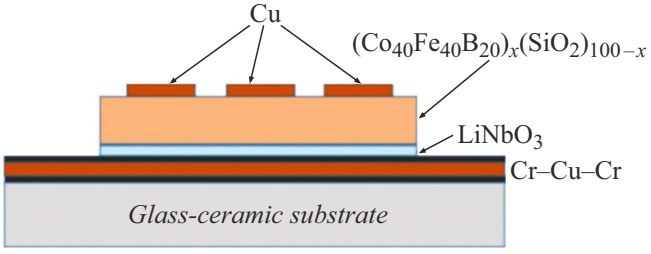

Figure 1. Topology of the experimental samples M/NC/D/M.

NC was deposited using a similar technology. The composite target was a $Co_{40}Fe_{40}B_{20}$ alloy plate with a size of 280 × 80 × 10 mm, on the surface of which 13 subsamples of a single crystal quartz with a size of 80 × 10 × 2 mm were attached. The location of the subsamples was uneven along the length of the target. This made it possible to smoothly and continuously change the concentration of the metal phase of the composite on the surface of the substrates depending on the arrangement of the substrate-target [24,25]. For more complete oxidation of the dielectric phase of NC during synthesis, a small amount of oxygen of the order of $0.9 \cdot 10^{-5}$ Torr partial pressure was added to the inert gas (Ar) at a pressure of $3.9 \cdot 10^{-4}$ Torr. The chosen configuration of the composite target and the number of attachments made it possible to vary the concentration of the metal phase of the composite from 18.9 to 42.1 at.%, depending on the position of the samples during deposition. Sputtering was carried out for 15 min at an anode voltage of 2 kV and a plasma current of 100 mA on a fixed substrate. This made it possible to form a film of HC with a thickness of ≈ 250 nm. As in the case of applying the lower electrode, ion cleaning of the substrate surface was carried out before spraying.

The upper copper contact pads were applied through a metal mask with a hole size of 0.5 × 0.2 mm for 30 min using the technology described above.

The ion beam vacuum spraying unit has an oil-free pumping system consisting of spiral and turbomolecular pumps. A vacuum of no worse than $1.0 \cdot 10^{-6}$ Torr was created before spraying. Extremely pure gases of no worse than 99.999 % were used for the synthesis.

The elemental composition of NCs was determined using an Oxford INCA Energy 250 energy-dispersive X-ray attachment on a JEOL JSM-6380 LV scanning election microscope. The structural analysis was performed by X-ray method using BRUKER D2 PHASER X-ray diffractometer.

The volt-ampere characteristics (VAC) of structures $Cu/(CoFeB)_x(SiO_2)_{100-x}/LiNbO_3$/Cr–Cu–Cr/polycrystalline glass and their memristive properties were measured using a multifunctional KEITHLEY 2450 measuring source and an analytical probe station in current limiting mode. VAC of structures MNC/M were measured with grounded bottom electrode and bias voltage sweep U of top electrode as per linear law in sequence from

$0 \to +U_{max} \to U_{max} \to 0$ V with step 0.1 V. The rate of voltage change was 10 V/s.

2. Experimental results

13 cells of a memristive structure were synthesized in the course of the study, differing in the concentration of the metal phase in the composite in the range from 18.9 to 42.1 at.%. Figures 2 and 3 show, respectively, diffraction patterns of films of NC $(CoFeB)_x(SiO_2)_{100-x}$ and VAC of memristive elements for intermediate concentrations, which most clearly demonstrate the dynamics of memristive properties.

The characterization of the structure of NC $(CoFeB)_x(SiO_2)_{100-x}$ and D $LiNbO_3$ was performed by X-ray method on films of the order of 1 μm thick deposited on the surface of single-crystal Si (100).

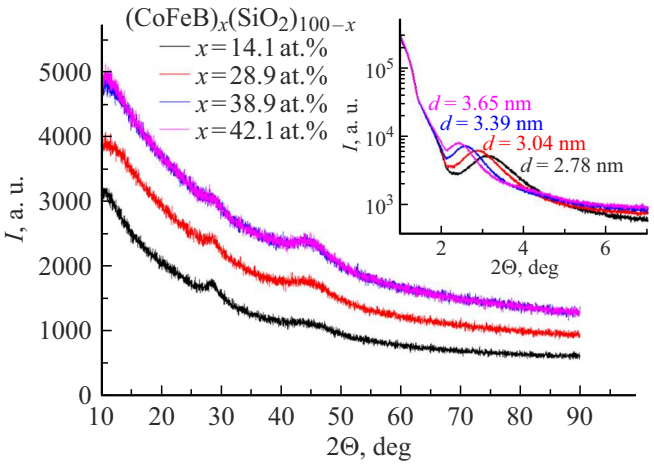

Figure 2. Diffraction patterns of films of NC $(CoFeB)_x(SiO_2)_{100-x}$.

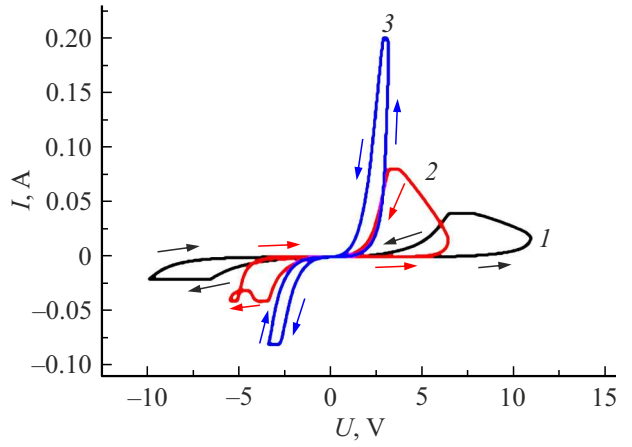

Figure 3. VAC of the memristive element $Cu/(Co_{40}Fe_{40}B_{20})_x(SiO_2)_{100-x}/LiNbO_3/Cr/Cu/Cr/$polycrystalline glass at different concentrations of the metallic phase of NC: *1* — 18.9, *2* — 35.5, *3* — 41.9 at.%.

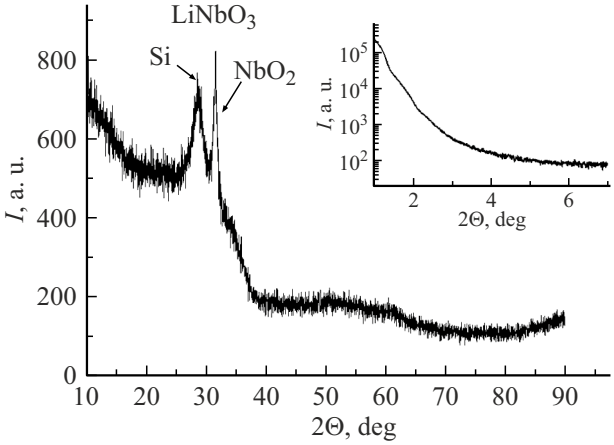

Figure 4. Diffraction pattern of the $LiNbO_3$ film.

X-ray diffraction did not reveal the crystal structure of NC in the entire range of concentrations of the metal phase under consideration (Fig. 2). It is remarkable that small-angle X-ray diffraction is observed in films of NC $(CoFeB)_x(SiO_2)_{100-x}$. This phenomenon is possible if we assume that the NC has a fairly well-ordered structure of the relative arrangement of metal granules. The average distance between the granules can be estimated from the position of the maximum. It is on the order of 3 nm and increases with increasing concentration of the metal phase (Fig. 2, insert).

X-ray diffraction from the $LiNbO_3$ film (Fig. 4) is most accurately described when it is modeled by a medium where niobium oxide nanocrystals are embedded in an amorphous matrix. The position of the peak suggests that niobium oxide is closer to the unsaturated form of Nb_2O_5. The absence of small-angle diffraction may indicate the absence of an ordered distribution of niobium oxide nanoparticles or their large (> 8 nm) size (Fig. 4, box).

Bipolar resistive switching is observed throughout the studied concentration range as can be seen on the VAC curves of the structures of $Cu/(Co_{40}Fe_{40}B_{20})_x(SiO_2)_{100-x}/LiNbO_3/Cr/Cu/Cr/$polycrystalline glass shown in Fig. 4. The switching voltage from the high-resistance to the low-resistance state ($R_{off} \to R_{on}$) and from the low-resistance to the high-resistance state ($R_{on} \to R_{off}$) differ significantly depending on the concentration of the metal phase in the NC. Besides, as value x increases, the current through the specimen, where RS are observed, increases. These parameters, as well as the ratio R_{off}/R_{on} depending on the concentration of the metallic phase of NC, are shown in Fig. 5. The range of x can be distinguished, within which optimal properties of structures are observed. Switching voltage in the region of ± 4 V and the ratio of $R_{off}/R_{on} \approx 50$.

A more detailed analysis of the concentration dependences of the memristive properties for the structure $Cu/(Co_{40}Fe_{40}B_{20})_x(SiO_2)_{100-x}/LiNbO_3/Cr/Cu/Cr/$ polycrystalline glass is shown in Fig. 5.

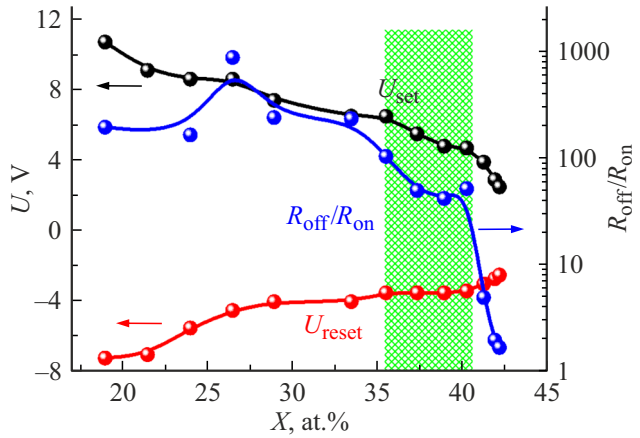

Figure 5. Concentration dependences of parameters R_{off}/R_{on}, U_{set} and U_{reset} for the Cu/$(Co_{40}Fe_{40}B_{20})_x(SiO_2)_{100-x}$/$LiNbO_3$/Cr/Cu/Cr/polycrystalline glass.

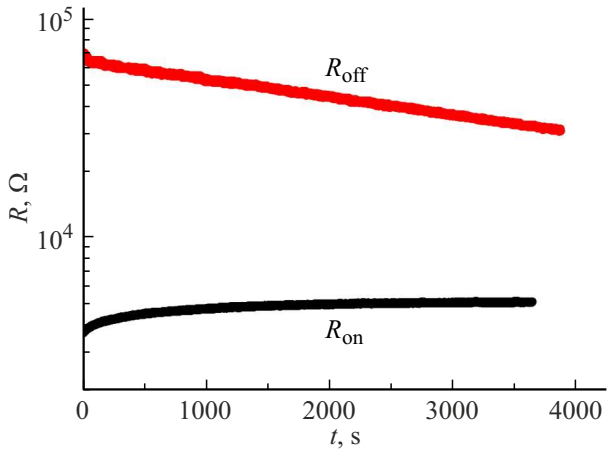

Figure 6. Time dependence of induced resistive states for memristor structures Cu/$(Co_{40}Fe_{40}B_{20})_{35.5}(SiO_2)_{64.5}$/$LiNbO_3$/Cr/Cu/Cr/polycrystalline glass.

3. Analysis of findings

Taking into account the mechanism of the multifilament RS in the $LiNbO_3$ dielectric layer, which is determined by conducting channels in the NC, it is easy to explain the results obtained. As the concentration of the metal phase in NC $(Co_{40}Fe_{40}B_{20})_x(SiO_2)_{100-x}$ increases, both a decrease in channel resistance (R_{ch}) and an increase in density are observed conducting channels. A decrease in R_{ch} leads to a redistribution of voltage in the channel-dielectric chain and, consequently, an increase in voltage across the $LiNbO_3$ layer, which causes RS. Current through the specimen is specified by density of induced filaments, which is proportionate to the density of conducting channels in NC.

A significant property of memristors is the preservation of induced resistive states over time. This characteristic tends to relax in the studied memristive structures (Fig. 6). We observed similar behavior in structures where $(Co_{40}Fe_{40}B_{20})_x(LiNbO_3)_{100-x}$ was used as the NC [26]. It was shown in this study that the thermal activation of electrons from neutral vacancies into the impurity zone and the hopping transfer of charges in it play an essential role in the relaxation of the induced resistive state. Since the identified relaxation processes in $LiNbO_3$ have different τ_0 and E_{act}, a pulse RS algorithm has been developed in which the processes responsible for relaxation of the induced resistive state do not have time to be implemented [27].

A measurement of quasi-static VAC was performed to study the issue of low temporal stability of induced resistive states. Voltage step was 0.1 V. 10 current resistance values were measured at the current voltage for 10 s (Fig. 7). These values were treated by calculation of relative change in resistance at fixed voltage on sample (Fig. 8).

In the region of positive voltages applied to the upper electrode, irreversible changes in the resistive state (decrease in values R) are observed at very low voltages and

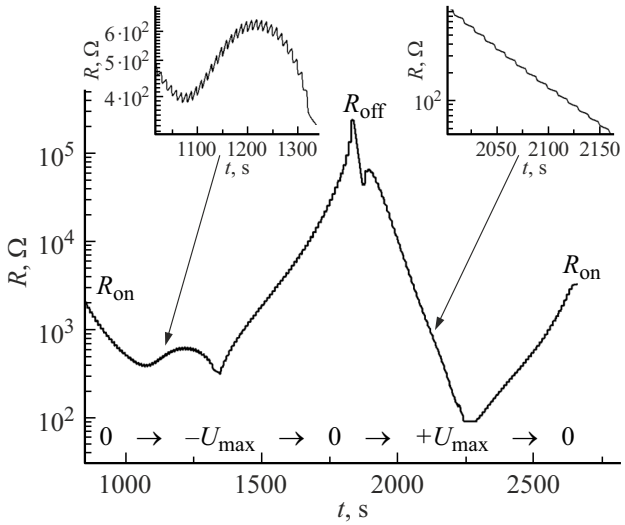

Figure 7. Time dependence of the change in the resistance of the Cu/$(Co_{40}Fe_{40}B_{20})_{35.5}(SiO_2)_{64.5}$/$LiNbO_3$/Cr/Cu/Cr/polycrystalline glass when the applied voltage changes.

continue at an increasing rate up to ∼ 3.5 V. It is easy to imagine this dependence $(R_{i+1}-R_i)/R_i)$ as a superposition of two processes of resistance change under the action of applied voltage, implemented in a different range of applied potential. No significant voltage changes are observed during the transition $R_{on} \rightarrow R_{off}$ in the range from 0 to −2 V. The structure is switched to a high-resistance state in the voltage range from −2 to −4 V, which correlates well with the course of time dependence of induced resistive states (Fig. 7).

We observe a similar pattern on the family of curves $R(t)$, which demonstrates the plasticity of induced resistive states (the ability to realize any resistance value of the structure between R_{off} and R_{on}) (Fig. 9). It can be seen that the nominal value decreases during the measurement time in

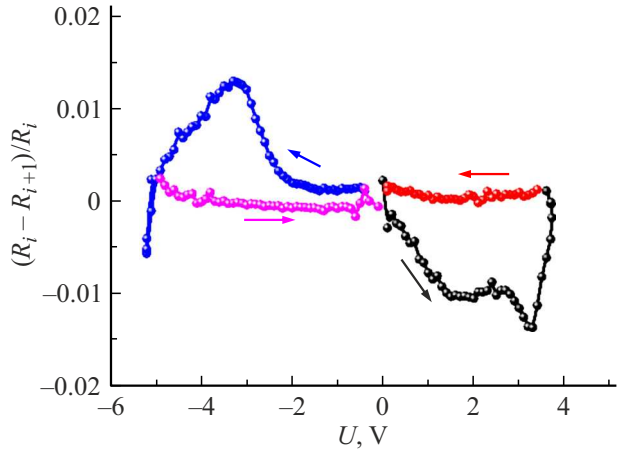

Figure 8. Relative rate of change of resistance for $Cu/(Co_{40}Fe_{40}B_{20})_{35.5}(SiO_2)_{64.5}/LiNbO_3/Cr/Cu/Cr/$polycrystalline glass from applied voltage.

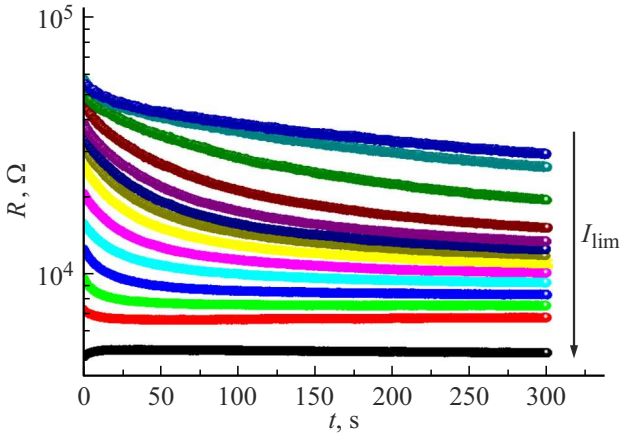

Figure 9. Time dependence of the resistive states of memristor structures $Cu/(Co_{40}Fe_{40}B_{20})_{35.5}(SiO_2)_{64.5}/LiNbO_3/Cr/Cu/Cr/$ polycrystalline glass induced at various limiting currents.

case of relatively large values of R , whereas $R(t)$ increases at values R close to the minimum. This is consistent with the curves in Fig. 6. At the same time, the rate of decrease of $R(t)$ is higher than the increase of $R(t)$.

Nevertheless, the structures of $Cu/(Co_{40}Fe_{40}B_{20})_x(SiO_2)_{100-x}/LiNbO_3/Cr/Cu/Cr/$polycrystalline glass exhibit significant stability of reversible RS (Fig. 10). The parameters of the switching pulses (pulse voltage, pulse current, and pulse time) are shown in the figure. Degradation of induced states is not observed after 10^4 switching cycles.

Conclusion

Studies of the complex of memristic properties of $Cu/(Co_{40}Fe_{40}B_{20})_x(SiO_2)_{100-x}/LiNbO_3/Cr/Cu/Cr/$ polycrystalline glass structure have shown that reversible bipolar switching is observed in the range of concentrations of the metallic phase of NC from 18 to 43 at.%. The

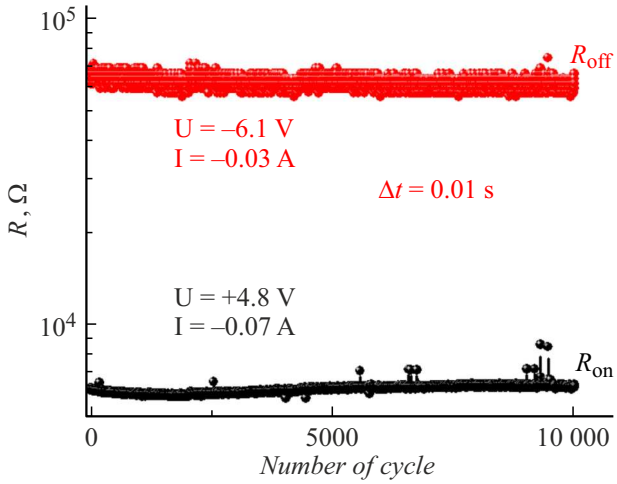

Figure 10. Switching of resistive states in memristor structures $Cu/(Co_{40}Fe_{40}B_{20})_{35.5}(SiO_2)_{64.5}/LiNbO_3/Cr/Cu/Cr/$polycrystalline glass.

magnitude of the switching voltages from R_{off} to R_{on} states and, conversely, decreases with increase of x and reaches ± 4 V at $x = 37$ at.R_{off}/R_{on} reaches hundreds of units. The number of cycles of reversible RS is more than 10^4. Some relaxation of the time dependences of the induced resistive states has been revealed, which is related to the electrical properties of the functional layer $LiNbO_3$, which in its initial state is a complex heterogeneous structure where nanocrystals NbO_2 are embedded in an amorphous matrix. A comprehensive study has confirmed that in order to implement a multifilament RS in a dielectric layer, the presence of NC with a concentration of the metal phase is necessary before the percolation threshold between the upper and lower electrodes. In this case, the main role is played by the NC structure, and the elemental composition of the heterogeneous film is not so essential for the implementation of the complex of technologically significant properties of the memristor.

Funding

This study was financially supported by the Russian Science Foundation, project № 25-29-00215.

Conflict of interest

The authors declare that they have no conflict of interest.

References

[1] D. Ielmini. Semicond. Sci. Technol, **31**, 063002 (2016). DOI: 10.1088/0268-1242/31/6/063002
[2] W. Banerjee, Q. Liu, H. Hwang. J. Appl. Phys., **127**, 051101 (2020). DOI: 10.1063/1.5136264
[3] Y. Zhang, Z. Wang, J. Zhu, Y. Yang, M. Rao, W. Song, Y. Zhuo, X. Zhang, M. Cui, L. Shen, R. Huang, J. Yang. Appl. Phys. Rev., **7**, 011308 (2020). DOI: 10.1063/1.5124027

[4] D. Ham, H. Park, S. Hwang, K. Kim. Nat. Electron., **4**, 635 (2021). DOI: 10.1038/s41928-021-00646-1
[5] Q. Xia, J.J. Yang. Nat. Mater., **18**, 309 (2019). DOI: 10.1038/s41563-019-0291-x
[6] M. Zhuk, S. Zarubin, I. Karateev, Y. Matveyev, E. Gornev, G. Krasnikov, D. Negrov, A. Zenkevich. Front. Neurosci., **14**, 94 (2020). DOI: 10.3389/fnins.2020.00094
[7] B.S. Shvetsov, A.V. Emelyanov, A.A. Minnekhanov, V.V. Rylkov, V.A. Demin. Nanotechnol. Russia., **16**, 777 (2021). DOI: 10.1134/S2635167621060239
[8] Z. Wang, H. Wu, G.W. Burr, C.S. Hwang, K.L. Wang, Q. Xia, J.J. Yang. Nature Rev. Mater., **5**, 173 (2020). DOI: 10.1038/s41578-019-0159-3
[9] G.A. Yuklyaevskikh, B.S. Shvetsov, A.V. Emelyanov, V.A. Kulagin, V.V. Rylkov, V.A. Demin. Chaos, Solitons Fractals, **190**, 115784 (2025). DOI: 10.1016/j.chaos.2024.115784
[10] Y. Li, Z. Wang, R. Midya, Q. Xia, J.J. Yang. J. Phys. D: Appl. Phys., **51**, 503002 (2018). DOI: 10.1088/1361-6463/aade3f
[11] D.-H. Kwon, K.M. Kim, J.H. Jang, J.M. Jeon, M.H. Lee, G.H. Kim, X.-S. Li, G.-S. Park, B. Lee, S. Han, M. Kim, C.S. Hwang. Nat. Nanotechnol., **5**, 153 (2010). DOI: 10.1038/nnano.2009.456
[12] J.-Y. Chen, C.-W. Huang, C.-H. Chiu, Y.-T. Huang, W.-W. Wu. Adv. Mater., **27**, 5028 (2015). DOI: 10.1002/adma.201502758
[13] H. Jiang, L. Han, P. Lin, Z. Wang, M.H. Jang, Q. Wu, M. Barnell, J.J. Yang, H.L. Xin, Q. Xia. Sci. Rep., **6**, 28525 (2016). DOI: 10.1038/srep28525
[14] V.V. Rylkov, S. Nikolaev, V.A. Demin, A.V. Emelyanov, A.V. Sitnikov, K.E. Nikiruy, V.A. Levanov, M.Yu. Presnyakov, A.N. Taldenkov, A.L. Vasiliev, K.Yu. Chernoglazov, A. Vedeneev, Yu.E. Kalinin, A.B. Granovsky, V. Tugushev, A.S. Bugaev. J. Exp. Theor. Phys., **126**, 367 (2018). DOI: 10.1134/S1063776118020152
[15] V.A. Levanov, A.V. Emel'yanov, V.A. Demin, K.E. Nikirui, A.V. Sitnikov, S.N. Nikolaev, A.S. Vedeneev, Yu.E. Kalinin, V.V. Rylkov. J. Commun. Technol. Electron., **63**, 496 (2018). DOI: 10.1134/S1064226918050078
[16] K.E. Nikiruy, A.V. Emelyanov, V.A. Demin, A.V. Sitnikov, A.A. Minnekhanov, V.V. Rylkov, P.K. Kashakrov, M.V. Kovalchuk. AIP Advances, **9**, 065116 (2019). DOI: 10.1063/1.5111083
[17] A.V. Emelyanov, K.E. Nikiruy, A.V. Serenko, A.V. Sitnikov, M.Yu. Presnyakov, R.B. Rybka, A.G. Sboev, V.V. Rylkov, P.K. Kashkarov, M.V. Kovalchuk. Nanotechnology, **31**, 045201 (2020). DOI: 10.1088/1361-6528/ab4a6d
[18] K.E. Nikiruy, I.A. Surazhevsky, V.A. Demin, A.V. Emelyanov. Phys. Status Solidi A, **217** (18), 1900938 (2020). DOI: 10.1002/pssa.201900938
[19] I.A. Surazhevsky, V.A. Demin, A.I. Ilyasov, A.V. Emelyanov, K.E. Nikiruy, V.V. Rylkov, S.A. Shchanikov, I.A. Bordanov, S.A. Gerasimova, D.V. Guseinov, N.V. Malekhonova, D.A. Pavlov, A.I. Belov, A.N. Mikhaylov, V.B. Kazantsev, D. Valenti, B. Spagnolo, M.V. Kovalchuk. Chaos, Solitons Fractals, **146**, 110890 (2021). DOI: 10.1016/j.chaos.2021.110890
[20] V.V. Rylkov, S.N. Nikolaev, K.Y. Chernoglazov, V.A. Demin, M.Y. Presnyakov, A.L. Vasiliev, V.V. Tugushev, A.B. Granovsky, A.V. Sitnikov, Y.E. Kalinin, N.S. Perov, A.S. Vedeneev. Phys. Rev. B, **95** (14), 144202 (2017). DOI: 10.1103/PhysRevB.95.144202
[21] A.V. Sitnikov, I.V. Babkina, Yu.E. Kalinin, A.E. Nikonov, M.N. Kopytin, A.R. Shakurov, O.I. Remizova, L.I. Yanchenko. ZhTF, **92** (9), 1382 (2022) (in Russian). DOI: 10.21883/JTF.2022.09.52930.94-22
[22] A.V. Sitnikov. Materialovedenie, **3**, 49 (2010). (in Russian)
[23] S.A. Gridnev, Yu.E. Kalinin, A.V. Sitnikov, O.V. Stogney. *Nelineynye yavleniya v nano- i mikrogeterogennykh sistemakh* (BINOM, Laboratoriya znaniy, M., 2012) (in Russian)
[24] Yu.E. Kalinin, A.N. Remizov, A.V. Sitnikov. Phys. Solid State, **46** (11), 2146 (2004). DOI: 10.1134/1.1825563
[25] N. Domracheva, M. Caporali, E. Rentschler. *Novel Magnetic Nanostructures: Unique Properties and Applications* (Elsevier, 2018)
[26] A.V. Sitnikov, A.V. Yemelyanov, A.E. Nikonov, K.E. Nikitui, K.Y. Chernoglazov, D.V. Ichetkin, A.I. Ilyasov, S.N. Nikolaev, V.A. Demin, A.S. Vedeneev, Yu.E. Kalinin, V.V. Rylkov. V sb.: Materialy XXVI Mezhdunarodnogo simpoziuma „Nanofizika i nanoelektronika", pod red. M.L. Timoshenko, V.V. SHeina (Izd-vo Nizhegorodskogo gos. un-ta im. N.I. Lobachevskogo, Nizhnij Novgorod, 2022), p. 362 (in Russian).
[27] K.E. Nikiruy, A.V. Yemelyanov, V.A. Demin, V.V. Rylkov, A.V. Sitnikov, P.K. Kashkarov. Pisma v ZhTF **44**, 28 (2018) (in Russian). DOI: 10.21883/PJTF.2018.10.46095.17099

Translated by A.Akhtyamov